DENSITY FUNCTIONAL THEORY CALCULATION AND RAMAN SCATTERING OF THE ANTIHISTAMINE EBASTINE

H. Peng, D.-X. Wu, H.-Y. Hou, X.-B. Chen*

Hubei Key Laboratory of Optical Information and Pattern Recognition,
Wuhan Institute of Technology, Wuhan 430205, China; e-mail: xchen@wit.edu.cn

The vibrational properties of ebastine have been investigated by density functional theory (DFT) calculations and Raman scattering experiments. The DFT calculation was performed with geometry optimization and harmonic vibration using the B3LYP function with the 6-31G(d) basis set. The DFT calculated spectrum of ebastine is in good agreement with Raman scattering experiments. A good linear correlation between calculated and experimental wavenumbers has been obtained in the spectral range of 500–3250 cm^{-1}. Also, the calculated bond lengths and bond angles of the ebastine molecule are consistent with reported X-ray diffraction results. The deviations of bond lengths and bond angles are smaller than 0.034 Å and 3.1°, respectively. In addition, the experimentally observed vibrational modes have been assigned and the characteristic modes of the three parts benzhydryloxy, piperidine-butanone, and tert-butylphenyl of the ebastine molecule have been discussed, which would be helpful for future degradation and activity studies of ebastine.

Keywords: *ebastine, density functional theory calculation, Raman scattering, vibrational states.*

СПЕКТРЫ КОМБИНАЦИОННОГО РАССЕЯНИЯ АНТИГИСТАМИННОГО ПРЕПАРАТА ЭБАСТИНА И ИХ РАСЧЕТ С ПОМОЩЬЮ ТЕОРИИ ФУНКЦИОНАЛА ПЛОТНОСТИ

H. Peng, D.-X. Wu, H.-Y. Hou, X.-B. Chen*

УДК 535.375.5;539.194

Уханьский технологический институт,
Ухань, 430205, Китай; e-mail: xchen@wit.edu.cn

(Поступила 3 июня 2019)

Колебательные свойства эбастина исследованы с помощью теории функционала плотности (DFT) и методов комбинационного рассеяния. Расчет на основе DFT выполнен с оптимизацией геометрии и в предположении гармоничности колебаний с помощью функции B3LYP с базисным набором 6-31G(d). Рассчитанный с помощью DFT спектр эбастина хорошо согласуется с экспериментальным спектром КР. Получена хорошая линейная корреляция между рассчитанными и измеренными частотами в диапазоне 500—3250 см$^{-1}$. Рассчитанные длины углы связей молекулы эбастина согласуются с результатами рентгеновской дифракции, отклонения расчетных значений от экспериментальных <0.034 Å и 3.1°. Сделано отнесение экспериментальных колебательных мод и обсуждены характерные моды трех составляющих молекулы эбастина — бензгидрилокси, пиперидин-бутанона, трет-бутилфенила.

Ключевые слова: *эбастин, расчет с помощью теории функционала плотности, комбинационное рассеяние, колебательные состояния.*

Introduction. Ebastine, a second-generation H_1 receptor antagonist, is commonly used for symptomatic treatment of allergic rhinitis and urticaria [1–3]. It does not penetrate the blood–brain barrier to a significant amount, thus has low risk of side effects, such as sedation or drowsiness [4, 5]. Also, low side effects of a high dose of ebastine in a child have been reported [6]. The pharmacologically active metabolite, carebastine, is formed by the oxidation at methyl carbon on the tert-butyl group of the ebastine molecule [7]. Thus, knowledge of molecular vibrational properties, especially that involving the tert-butyl group, would be helpful for identifying and understanding the activity of ebastine. Also, a recent study showed that ultraviolet (UV) radiation

can cause degradation of ebastine [8]. Knowledge of molecular vibrational properties would be useful for understanding the UV degradation of ebastine.

Raman scattering is a powerful technique to investigate vibrational properties of molecules. However, for large molecules, it is difficult to have a good understanding of vibrational properties by Raman scattering solely. In this paper, we combine Raman scattering experiment and DFT calculation to investigate the molecular vibrational properties of the antihistamine ebastine. Good agreement between DFT calculation and Raman scattering experiment has been achieved with one scaling factor 0.9591±0.0020 in the spectral range 500–3250 cm^{-1}. This scaling factor is consistent with the reference scaling factor 0.9614 [9]. Also, a good linear relation with R^2 of 0.99985 has been obtained, and the deviations are smaller than 36 cm^{-1}. In addition, the bond lengths and bond angles of the ebastine molecule have been calculated, and the values are consistent with reported X-ray diffraction results. Furthermore, the characteristic vibrational modes of the three parts benzhydryloxy, piperidine-butanone, and tert-butylphenyl of the ebastine molecule have been assigned and discussed.

Experiment and computational method. The powder form of the ebastine sample was purchased from TCI (Shanghai) Development Company with a stated purity greater than 98% and used as received without further purification. Raman scattering measurements of the ebastine sample were performed in backscattering configuration with a Thermo Fisher DXR micro-Raman spectrometer. Two excitation lasers of 532 and 633 nm were used. The scattered signal was detected by an air-cooled CCD detector. The spectra were corrected in wavenumber by using the 521 cm^{-1} vibrational mode of a Si substrate.

For the DFT calculation, we employed the commonly applied method of Becke's [10, 11] exchange function in combination with Becke's three-parameter hybrid exchange function using the LYP [12, 13] correlation function of Lee, Yang, and Parr (B3LYP). The polarized 6-31G(*d*) basis set was used for geometry optimization and analytical vibration frequency calculation. The quantum mechanical calculations were performed using the ORCA program [14]. By using the VEDA 4 program [15, 16] for the related molecules, the vibrational wavenumber assignments were made with a high degree of accuracy. Calculated data analysis and graph plotting were performed using the Multiwfn_3.4.1(dev) program [17]. The Lorentzian curve was chosen for the line shape and 8 cm^{-1} was chosen for the full width at half maximum of each peak.

Results and discussion. Figure 1 presents the Raman scattering of the ebastine sample with two excitation lasers of 532 and 633 nm in the spectral range of 500–3200 cm^{-1}. As can be seen in Fig. 1, the vibrational modes of ebastine can be much more easily observed by green laser than red laser, since Raman scattering intensity is generally inversely proportional to the fourth power of excitation laser wavelength. There are 38 vibrational modes that can be resolved in the spectral range of 500–3200 cm^{-1} in Fig. 1. Ebastine has the molecular formula of $C_{32}H_{39}NO_2$, with molecular structure as shown in Fig. 2. In the figure, the complex molecular structure is divided into three parts A, B, and C. Due to large molecular formula and complex molecular structure of ebastine, the assignment of the crowded vibrational modes in Fig. 1 is difficult. Below we will apply DFT calculation and compare in detail with the experimental result for the assignment of all the 38 observed vibrational modes.

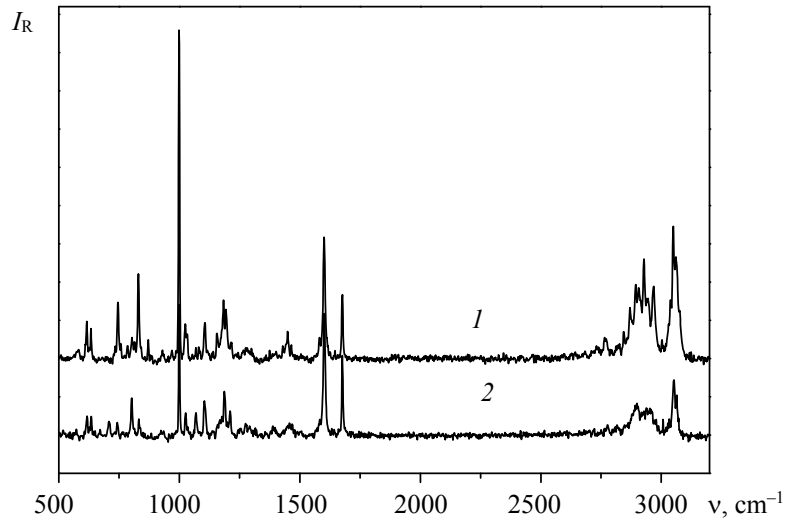

Fig. 1. Raman scattering of ebastine with 532 (1) and 633 nm (2) laser excitations.

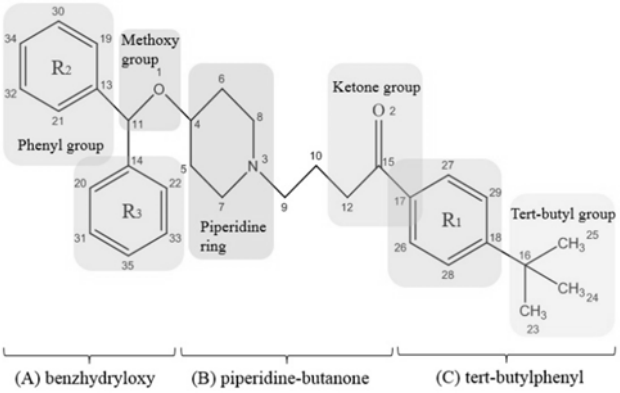

Fig. 2. Molecular structure of ebastine; benzhydryloxy, piperidine-butanone, and tert-butylphenyl — parts A, B, and C, respectively.

To achieve accurate vibrational frequency calculation, the ground-state geometry of the ebastine molecule was optimized at the B3LYP/6-31G(*d*) level of theory without any symmetry restrain. The calculated result showed that there is no imaginary frequency, indicating that the optimized geometry is at the lowest point of the potential energy surface. The calculated bond lengths and bond angles of the ebastine molecule are presented in Tables 1 and 2, respectively. As can be seen, our calculated results are consistent with the reported experimental bond lengths and bond angles obtained with X-ray diffraction [18]. The deviations of bond lengths and bond angles are smaller than 0.034 Å and 3.1°, respectively.

TABLE 1. DFT Calculated Bond Lengths (Å) of Ebastine Molecule in Comparison with the XRD Results

Bond	Calculated	Ref. [18]
C21-C32	1.397	1.376
C21-C13	1.398	1.383
C32-C34	1.394	1.368
C34-C30	1.396	1.366
C30-C19	1.394	1.376
C19-C13	1.402	1.379
C13-C11	1.529	1.513
C11-O1	1.424	1.427
C4-O1	1.433	1.430
C4-C5	1.534	1.500
C4-C6	1.528	1.506
C5-C7	1.545	1.515
C7-N3	1.467	1.459
C8-N3	1.464	1.456
C8-C6	1.542	1.507
C12-C15	1.529	1.482
C15-O2	1.224	1.221
C15-C17	1.489	1.481

To obtain small deviations and good linear correlation between calculated and experimental wavenumbers, the calculated wavenumbers are normally scaled down with some specific factors. In this study, the calculated wavenumbers of all the vibrational modes in the spectral range of 500–3250 cm^{-1} have been scaled down by a uniform scaling factor of 0.9591(±0.0020), which is obtained by linear fitting of the experimental and calculated wavenumbers using the Origin program. This value is consistent with the reference scaling factor 0.9614 [9]. Figures 3a and b present a comparison of Raman scattering experiment and DFT calculation in the spectral range of 500–1750 cm^{-1} and 2750–3250 cm^{-1}, respectively. The correlation of experimental and calculated wavenumbers is plotted in Fig. 4 and fitted with a linear line. Our results show that the deviations are less than 36 cm^{-1} between calculated and experimental wavenumbers, and all the modes provide a good linear correlation between calculated and experimental wavenumbers with R^2 of 0.99985.

TABLE 2. DFT Calculated Bond Angles (degree) of Ebastine Molecule in Comparison with the XRD Results

Bond	Calculated	Ref. [18]
C32-C21-C13	120.4	121.2
C34-C32-C21	120.4	119.8
C30-C34-C32	119.4	119.9
C34-C30-C19	120.2	120.2
C30-C19-C13	120.7	121.0
C19-C13-C11	120.0	121.6
C21-C13-C11	121.2	120.4
O1-C4-C5	107.5	108.7
O1-C4-C6	112.0	112.2
C5-C4-C6	110.3	109.3
C4-C5-C7	110.7	110.7
N3-C7-C5	114.2	111.2
N3-C8-C6	114.5	112.2
C4-C6-C8	110.3	110.6
N3-C9-C10	111.7	114.8
C9-C10-C12	113.0	111.9
O2-C15-C17	120.4	119.4
O2-C15-C12	120.8	120.1

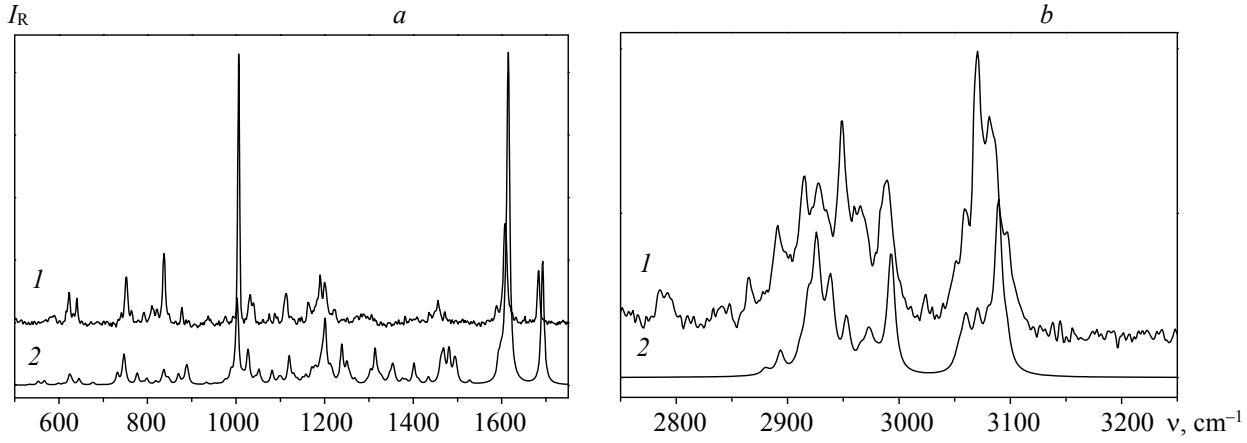

Fig. 3. Comparison of Raman scattering spectrum and DFT calculated spectrum in the spectral range of 500–1750 cm^{-1} (a) and 2750–3250 cm^{-1} (b), 1 – experimental, 2 – calculated.

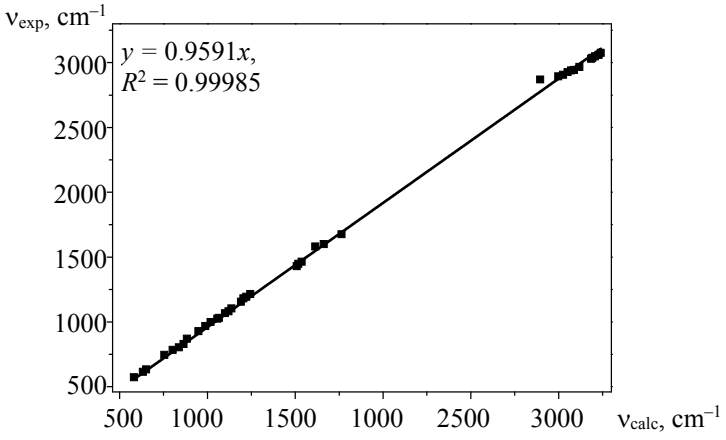

Fig. 4. The linear fit of DFT calculated and Raman experimental wavenumbers.

The vibrational mode assignments have been performed by comparing the Raman observed peaks with DFT calculated wavenumbers; the results are presented in Table 3. The ebastine molecule has three parts, i.e., benzhydryloxy, piperidine-butanone, and tert-butylphenyl, which are labeled A, B, and C in Fig. 2. All the Raman observed vibrational modes of ebastine will be classified into three groups based on the three parts of the ebastine molecule, and the characteristic modes of each group will be discussed. This will be helpful for future studies of ebastine, such as understanding the activity of ebastine, UV degradation of ebastine, etc.

TABLE 3. Experimental and Calculated Vibrational Modes (cm^{-1}) of Ebastine in the Range of 500–3250 cm^{-1}

Experimental	Calculated		Assignment (%PED)
	Scaled	Unscaled	
572[C]	558	581	β(C23C16C18)(11)+β(C18C16C25)(10)
616[A]	608	633	β(C19=C30C34)(26)+β(C13=C21C32)(10)
633[C]	625	651	{β(C18C29=C27)+β(C26=C17C27)+β(C28C26=C17)+β(C29=C27C17)}(77)
745[A]	725	755	τ(HC30C34C32)(14)+τ(HC32C34C30)(18)+τ(HC34C32C21)(15)
784[B]	770	802	{ν(N3C7)+ν(N3C8)+ν(N3C9)}(43)
	781	814	τ(HC10C12C15)(15)+τ(HC8N3C7)(10)
804[B,C]	804	838	ν(C5C4)(15)+τ(HC28C26C17)(14)
	815	849	τ(H6C28C26C17)(18)+τ(HC26C28C18)(25)
830[A]	829	864	τ(HC20C31C35)(30)+τ(HC22C33C35)(20)+τ(HC33C35C31)(30) +τ(HC31C35C33)(19)
870[A]	849	884	{β(O1C11C13)+β(C4O1C11)}(10)
	900	938	{ν(C24C16)+ν(C25C16)}(46)+{τ(HC24C16C23)+τ(HC25C16C23)}(17)
929[C]	911	949	{ν(C24C16)+ν(C25C16)+ν(C23C16)}(25)+τ(HC23C16C24)(12)
	939	978	{ν(C5C4)+ν(C6C4)}(12)+ν(C6C8)(24)
968[A]	948	988	β(C30H,C32H,C34H of R2)(48)
999[A]	977	1018	ν(C19C30)(12)+ν(C31C20)(13)+β(C19C30C34)(38)+β(C33C35C31)(16)
1024[C]	1014	1056	τ(H_3C23C16C24)(12)+{τ(H_2C24C16C23)+τ(H_2C25C16C23)}(13)
1031[B]	1022	1065	{ν(O1C4)+ν(O1C11)}(12)
1067[B]	1056	1100	{ν(N3C7)+ν(N3C8)+ν(N3C9)}(14)+{ν(C5C4)+ν(C4C6)+ν(C10C9)+ ν(C12C10)}(35)
1081[B]	1075	1120	{ν(C5C4)+ν(C6C4)+ν(C10C9)+ν(C12C10)}(32)
1104[C]	1092	1137	ν(C18C29)(21)+β(HC28C26)(12)+β(C18= C29C27)(10)
	1108	1154	ν(C28C26)(20)+{β(HC28C26)+β(HC26C28)+β(HC29C27)+ β(HC27C29)}(51)
1156[A]	1143	1191	{β(HC30C34)+β(HC31=C35)+β(HC32=C34)+β(HC33C35)}(34) +β(HC34=C32)(10)+β(HC35C33)(23)
1181[A]	1157	1205	{ν(C13=C21)+ν(C20=C14)+ν(C21C32)}(10)+{ν(C11C13)+ν(C14C11)}(25) +{β(HC19C30)+β(HC20C31)+β(HC21C32)+β(HC22=C33)}(27)
1193[C]	1173	1222	{ν(C28C26)+ν(C29C27)}(11)+{β(HC28C26)+β(HC29C27) +β(HC26C28)+β(HC27C29)}(53)
1215[B]	1194	1244	ν(C17C15)(10)+{β(HC28C26)+β(HC29C27)+β(HC27C29)}(16)
	1216	1267	ν(C17C15)(14)
	1236	1287	β(H_2C5C7)(27)+τ(H_2C6C8N3)(11)+o(C5C6O1C4)(12)
	1248	1300	{τ(H44C8N3C7)+τ(H_2C9N3C7)}(13)
	1292	1346	{β(HC5C7)+β(HC6C8)+β(HC9C10)}(10)+{τ(HC4O1C11) +τ(H_2C5C7N3) +τ(HC6C8N3)}(24)
	1307	1361	β(HC12C15)(19)+τ(HC9N3C7)(13)+τ(HC10C12C15)(13)
	1333	1389	{β(HC5C7)+β(HC6C8)+β(HC9C10)}(13)+{τ(HC6C8N3) +τ(H_2C7N3C8H)}(14)
	1351	1407	{β(HC4O1)+β(HC11O1)}(11)+{τ(HC4O1C11)+τ(HC5C7N3)}(25)
	1371	1428	{β(HC4O1)+β(HC11O1)}(37)
1429[B]	1448	1508	{β(C5H_2)+β(C6H_2)+β(C7H_2)+β(C8H_2)}(75)+{β(C9H_2)+β(C10H_2)}(10)

Continue Table 3

Experimental	Calculated		Assignment (%PED)
	Scaled	Unscaled	
1449[B]	1457	1518	{β(C5H$_2$)+β(C6H$_2$)+β(C7H$_2$)+β(C8H$_2$)}(79)
1464[C]	1476	1537	β(C23H$_3$)(55)+β(HC24H)(17)+β(HC23C16C24)(10)
1582[C]	1550	1615	{ν(C18C29)+ν(C26=C17)+ν(C28C26)+ν(C29=C27)}(28)+ν(C27C17)(28) +{β(HC28C26)+β(HC29=C27)+β(HC26C28)+β(HC27=C29)}(14) +{β(C18C29=C27)+β(C26=C17C27)+(C28C26=C17)+ (C29=C27C17)}(21)
1600[C]	1596	1663	{ν(C18C29)+ν(C26=C17)+ν(C28C26)+ν(C29=C27)}(53) +{β(HC28C26)+β(HC29=C27)+β(HC22C28)+β(HC27=C29)}(17)
1676[B]	1693	1764	ν(O2=C15)(87)
2870[A]	2863	2985	ν(C11H)(92)
2893[B]	2875	2998	ν$_a$(C9H$_2$)(81)
2906[B]	2901	3025	ν(C7H$_2$)(79)+ν(C8H)(10)
2927[C]	2926	3051	ν(C23H$_3$)(47)+ν(C24H$_3$)(42)+ν(C25H$_3$)(10)
2939[B]	2944	3070	ν(C10H$_2$)(10)+ν(C12H$_2$))65
2944[B]	2962	3088	ν(C6H)(10)+ν(C8H$_2$)(68)
2967[C]	2991	3118	νa(C23H$_3$)(57)+ν$_a$(C24H$_3$)(23)+νa(C25H$_3$)(11)
3030[A]	3055	3185	{ν(C30H)+ν(C32H)+ν(C34H)}71
3038[C]	3062	3192	ν(C28H)(49)+ν(C26H)(44)
3049[A]	3076	3207	{ν(C30H)+ν(C34H)}(67)+{ν(C32H)+ν(C19H)}(14)
3060[C]	3096	3228	ν(C27H)(45)+ν(C29H)(54)
3075[A]	3108	3240	ν(C21H)(97)

N o t e: Assignments and potential energy distribution (PED) (contribution ≥ 10%) for vibrational normal modes. Types of vibration: ν = stretching; τ = torsion; ν$_a$ = asymmetrical stretching; β = bending; o = out-of-plane bending. All wavenumbers are in cm^{-1}.

Part A of the ebastine molecule, benzhydryloxy, contains two benzene rings which are labeled R2 (C13, C19, C30, C34, C32, C21) and R3 (C33, C22, C14, C20, C31, C35), one C atom C11, and one O atom O1; R2, R3, and O1 are bound with C11. The observed modes at 616, 745, 830, 870, 968, 999, 1156, 1181, 2870, 3030, 3049, and 3075 cm^{-1} are correlated with vibrations of this part. In this part, the C11-O1 bond would be affected more significantly than other bonds when external perturbations or physical stimuli are applied. Thus, the identification of vibrational modes correlated with the C11-O1 bond would be helpful for future studies. Our results show that the two modes at 870 and 1031 cm^{-1} are correlated with the C11-O1 bond. The mode at 870 cm^{-1} is assigned to O1C11C13 and C4O1C11 bending. The mode at 1031 cm^{-1} is assigned to C11O1C4 stretching.

Part B of the ebastine molecule, piperidine-butanone, contains a piperidine ring with five C atoms (C4, C5, C6, C7, C8) and one N atom (N3), and a ketone chain of four C atoms (C9, C10, C12, C15) and one O atom (O2). The observed modes at 784, 804, 1031, 1067, 1081, 1215, 1429, 1449, 1676, 2893, 2906, 2939, and 2944 cm^{-1} are correlated with vibrations of this part. In part B, the C9-N3 bond would be affected more significantly than other bonds when external perturbations or physical stimuli are applied. Thus, the identification of vibrational modes correlated with the C9-N3 bond would be helpful for future studies. Our results show that the two modes at 784 and 1067 cm^{-1} are correlated with the C9-N3 bond. We expect that with UV irradiation, these two vibrational modes of ebastine will be mostly affected. The study of UV irradiation on ebastine is currently undergoing, and the results will be present elsewhere.

Part C of ebastine molecule, tert-butylphenyl, contains one benzene ring R1 (C17, C26, C28, C18, C29, C27) and four C atom (C16, C23, C24, C25). The observed modes at 572, 633, 804, 929, 1024, 1104, 1193, 1464, 1582, 1600, 2927, 2967, 3038, and 3060 cm^{-1} are correlated with vibrations of this part. It was reported that in the process of ebastine oxidization into the pharmacologically active metabolite carebastine, the methyl carbon on the tert-butyl group in part C is involved [7]. Thus, the identification of vibrational modes correlated with the methyl carbon (C23, C24, C25) would be helpful for understanding the activity of ebastine. Our results show that the three modes at 929, 1024, and 1464 cm^{-1} are correlated with the vibrations of methyl carbon. The mode at 929 cm^{-1} is correlated with the vibration of C16 with one methyl carbon. The mode

at 1024 cm^{-1} is correlated with H-C-C-C torsion, in which H and C atoms belong to the tert-butyl group. The mode at 1464 cm^{-1} is correlated with H-C bending in the methyl of the tert-butyl group.

Conclusions. The vibrational properties of the antihistamine ebastine have been investigated by DFT calculation and Raman scattering experiment. The DFT calculated spectrum of the ebastine molecule is in good agreement with Raman scattering experiments. The deviations of calculated and experimental wavenumbers are smaller than 36 cm^{-1}, and there is a good linear relation with R^2 of 0.99985. Also, the calculated bond lengths and bond angles of the ebastine molecule are consistent with reported X-ray diffraction results; the deviations are smaller than 0.034 Å and 3.1°, respectively. In addition, the experimentally observed vibrational modes have been assigned.

Acknowledgments. X. B. Chen acknowledges the support of the National Natural Science Foundation of China (Grant No. 11574241).

REFERENCES

1. F. Hampel, W. Howland, J. Van Bavel, P. Ratner, *J. Invest. Allergol. Clin. Immunol*., **14**, 56–63 (2004).
2. A. J. Moss, P. Chaikin, J. D. Garcia, M. Gillen, D. J. Roberts, J. Morganroth, *Clin. Exp. Allergy*, **29**, Suppl. 3, 200–205 (1999).
3. M. de Molina, A. Cadahia, L. Cano, A. Sanz, *Drug Invest*., **1**, 40–46 (1989).
4. M. Tagawa, M. Kano, N. Okamura, M. Higuchi, M. Matsuda, Y. Mizuki, H. Arai, R. Iwata, T. Fujii, S. Komemushi, *Br. J. Clin. Pharmacol*., **52**, 501–509 (2015).
5. J. Bousquet, E. Gaudaño, A. Palma Carlos, H. Staudinger, *Allergy*, **54**, 562–568 (2015).
6. L. Pecoraro, G. Paiola, A. Pietrobelli, *Clin. Case Rep*., **5**, 403–405 (2017).
7. M. Matsuda, Y. Mizuki, Y. Terauchi, *J. Chromatogr. B*, **757**, 173–179 (2001).
8. R. Rapolu, A. K. Pandey, C. K. Raju, K. Ghosh, K. Srinivas, A. Awasthi, S. G. Navalgund, K. V. Surendranath, *J. Pharm. Biomed. Anal*., **107**, 488–494 (2015).
9. A. P. Scott, L. Radom, *J. Phys. Chem.*, **100**, 16502–16513 (1996).
10. C. Lee, W. Yang, R. G. Parr, *Phys. Rev. B*, **37**, 785–789 (1988).
11. A. D. Becke, *Phys. Rev. A*, **38**, 3098–3100 (1988).
12. A. D. Becke, *J. Chem. Phys*., **98**, 1372–1377 (1993).
13. A. D. Becke, *J. Chem. Phys*., **104**, 1040–1046 (1996).
14. F. Neese, *The ORCA program system, Wiley Interdiscip. Rev. Comput. Mol. Sci*., **2**, 73–78 (2012).
15. M. H. Jamróz, *Spectrochim. Acta A*, **114**, 220–230 (2013).
16. M. H. Jamróz, *Vibrational Energy Distribution Analysis (VEDA)*, **4**, Warsaw (2004).
17. T. Lu, F. Chen, *J. Comput. Chem*., **33**, 580–592 (2012).
18. R. Sharma, D. Prasher, R. K. Tiwari, *J. Appl. Crystallogr*., **48**, 1299–1301 (2015).